PHILOSOPHICAL TRANSACTIONS OF THE ROYAL SOCIETY A MATHEMATICAL, PHYSICAL & ENGINEERING SCIENCES

A Review of Seasat Scatterometer Data

T. H. Guymer

Phil. Trans. R. Soc. Lond. A 1983 **309**, 399-414
doi: 10.1098/rsta.1983.0051

Phil. Trans. R. Soc. Lond. A **309**, 399–414 (1983)
Printed in Great Britain

A review of Seasat scatterometer data

By T. H. Guymer
Institute of Oceanographic Sciences, Brook Road, Wormley, Godalming, Surrey GU8 5UB, U.K.

A microwave scatterometer operating at 14.6 GHz was one of several sensors on Seasat that provided data at the sea surface. The technique by which estimates of the near-surface wind velocity can be obtained is described and studies to assess the accuracy of such data are reviewed. With few exceptions wind speed can be retrieved to ± 1.6 m s^{-1} and direction to $\pm 17°$ for winds between 3 and 16 m s^{-1}, and the technique is useful up to at least 25 m s^{-1}. The ability to measure wind on a near-global basis with a spatial resolution of 50 km is of great importance for meteorology and oceanography. Some examples of applications of scatterometer data are given, including the horizontal variation of the wind stress curl, the interpretation of synthetic aperture radar imagery and the inference of surface pressure fields. Comments on future satellite scatterometer systems are also made.

1. Introduction

One of the most important requirements for a better understanding of ocean circulation and improved weather forecasts is that of an adequate specification of the surface fluxes (Businger & Charnock 1983). In particular, improved knowledge of the surface wind field, which is the principal forcing function for the ocean, is essential to gaining an understanding of the variability of many of the world's surface current systems (O'Brien *et al.* 1982; Robinson 1963). Routine observations over the sea, obtained by conventional methods, lack the necessary spatial resolution, are concentrated in major shipping lanes and can have large errors due to poor calibration and exposure. Microwave remote sensing has developed over the past 10 years to the point where useful information about the wind near the sea surface can be obtained from a spacecraft at several hundred kilometres altitude. A major advance occurred when the first satellite dedicated to oceanography, Seasat-A, was launched by N.A.S.A. in 1978 (Born *et al.* 1981). It returned 100 days of data before a power failure occurred on 10 October, terminating the mission. Such was the volume of data obtained and its relevance to future microwave satellite sensors that extensive analysis still continues and is likely to do so for several years. Several scientific journals have produced issues dedicated to Seasat: *Science, Washington* (29 June 1979), *IEEE Journal of Oceanic Engineering* (April 1980), *Journal of Astronautical Sciences* (October–December 1980) and *Journal of Geophysical Research* (April 1982).

This paper assesses the capabilities of the Seasat-A Satellite Scatterometer (SASS) for measuring surface winds over the sea, in relation to its design specifications. Comparisons with surface measurements and with those from other Seasat sensors are used. Finally, examples of the applications of SASS data are described.

2. The Seasat scatterometer

(a) *Background*

Arising from radar research connected with World War II requirements, evidence emerged that backscatter from the ocean showed a dependence on surface winds (Cowan 1946; Kerr 1951; Grant & Yaplee 1957). Airborne measurements by the Naval Research Laboratory using a four-frequency radar (Daley 1973) and by N.A.S.A., operating a 13.3 GHz (Ku-band)

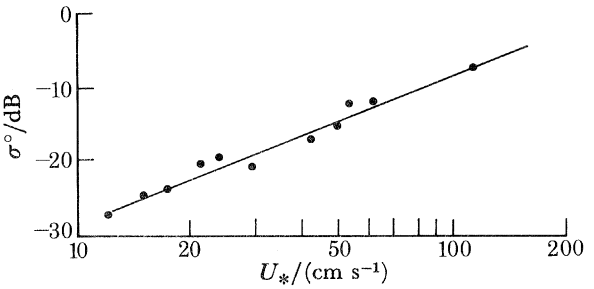

Figure 1. Variation of the normalized radar cross section, σ°, with friction velocity, U_*. Upwind, horizontally polarized measurements at an incidence angle of 40° from an airborne scatterometer have been used. (From Jones & Schroeder (1978).)

fan-beam scatterometer (Bradley 1971; Claasen *et al.* 1972) and a 'pencil-beam' 13.9 GHz combined microwave radiometer and scatterometer known as RADSCAT (Jones *et al.* 1977) enabled the dependence of backscatter on radar parameters and near-surface conditions to be quantitatively investigated. This led to the development of the first satellite-borne scatterometer (a mechanically scanned version of RADSCAT) launched on Skylab in 1973. The results all confirmed that the normalized radar cross section, σ°, depended on the wind speed; Guignard *et al.* (1971) suggested a simple power-law relation. Jones & Schroeder (1978) reanalysed the airborne RADSCAT data in terms of U_*, using Cardone's (1970) relation to derive the friction velocity, U_*, from wind and stability measurements (U_* is defined by $\rho U_*^2 = |\tau_0|$, where ρ is air density and τ_0 the surface shearing stress). An example of σ° as a function of U_* for particular values of incidence and azimuth angle, and horizontal polarization, is shown in figure 1.

The studies showed that higher radar frequencies (*ca.* 2 cm wavelength) were more sensitive to wind speed and that at these frequencies there were significant differences according to polarization. The variation with radar azimuth angle (off-nadir) was such that maxima occur in the upwind and downwind directions with minima close to crosswind, and this allows the possibility of recovering some directional information on the wind. At vertical incidence σ° was relatively insensitive to wind speed and the dependence was the reverse of that observed at 30–50°. A good review of these experimental results and of corresponding theoretical developments is contained in Moore & Fung (1979).

The data suggest that, for incidence angles greater than 25°, Bragg or resonant scattering is the dominant mechanism. At Ku-band frequencies the Bragg condition is satisfied for ocean waves of wavelength *ca.* 3 cm, i.e. in the short-gravity wave part of the spectrum. These ripples, which appear in light winds, grow in amplitude with increasing wind speed. However, the response of these short waves as wind speed continues to increase has been a source of some debate. Phillips (1977) has argued that saturation should occur at quite low speeds, the actual

PHILOSOPHICAL TRANSACTIONS OF THE ROYAL SOCIETY A MATHEMATICAL, PHYSICAL & ENGINEERING SCIENCES

value depending on how clean the surface is. In contrast Pierson & Stacy (1973) proposed a spectral form, based on data from a number of sources, which implied a strong wind-speed dependence of the capillary-gravity wave portion of the spectrum and this has been given some credence by Mitsuyasu (1977), who found a clear wind-speed response in measurements from a tower at wind speeds of 8 m s^{-1}. Both the aircraft backscatter and ocean wave data suggest that there is less sensitivity to wind for wavelengths greater than 5 cm. An additional complication is the effect of lower frequency waves on the short-gravity waves. Generally, it appears that a two-scale scattering model, in which it is assumed that Bragg scattering from small-scale roughness elements associated with local winds is modified by tilting due to the longer wave, is appropriate. A large degree of empiricism remains, though, in the specification of the relation between σ° and wind.

(*b*) *Wind-velocity determination*

The SASS (Grantham *et al.* 1977) was designed to view the ocean at two azimuths by using four dual-polarized fan-beam antennae aligned so that they pointed $\pm 45^\circ$ and $\pm 135^\circ$ in azimuth relative to the track beneath the satellite. Twelve Doppler filters were used to subdivide the antenna footprint electronically into resolution cells *ca.* 15 km (across beam) × 70 km (along beam). The incidence angles of the cells ranged from 25° to 55° for the regions illuminated by both forward and aft beams. Three additional measurements from incidence angles near nadir covered the subtrack, although no directional information can be obtained from them. Various operating modes of the SASS were used, allowing differing combinations of transmitted and received beam polarizations and swath coverage. Engineering aspects of SASS are discussed in detail by Johnson *et al.* (1980).

Two types of algorithm are needed before wind-velocity estimates are obtained. The first, the sensor algorithm (Bracalente *et al.* 1980), converts the basic engineering units to the normalized radar cross section, σ°. Corrections are made for the attenuation of the signal due to atmospheric water along the path by using the brightness temperature measured by the Seasat Scanning Multichannel Microwave Radiometer (SMMR). This can only be achieved for the swath to the right of the satellite track because of the look angle of the SMMR; no correction was made on the left-hand side. Moore *et al.* (1982) have attempted an evaluation of the attenuation algorithm and conclude that significant improvements in the wind determinations can be made in high precipitation rates.

From the σ° data the geophysical algorithm computes the 19.5 m neutral stability wind speed and direction. This is assumed to be the wind speed that would result from a given surface stress in near-neutral stratification and with a dry-adiabatic lapse rate from the surface to 19.5 m and avoids difficulties associated with the effect of air–sea temperature difference on the vertical variation of wind speed. Before the launch of Seasat three algorithms had been proposed (Pierson *et al.* 1974; Dome *et al.* 1977; Jones *et al.* 1978). As a result of comparisons with independent surface data these formulations were subsequently modified. The SASS model function $F(\theta_i, \phi, \epsilon, W)$ is empirical, relating the decadic logarithm of σ° to radar parameters and the surface wind vector, and is expressed by

$$F(\theta_i, \phi, \epsilon, W) = \lg \sigma^\circ = G(\theta_i, \phi, \epsilon) + H(\theta_i, \phi, \epsilon) \lg W, \quad (1)$$

where W is the wind speed, θ_i is the incidence angle, ϕ is the azimuth angle between the wind direction and the radar look angle, and ϵ is the polarization of the beam. The different model

functions are characterized by the values of G and H that they use for the various combinations of θ_1, ϕ and ϵ. A weighted least-squares method is used to find values for W and ϕ that, for a given model function, will produce the best fit to the observations of σ°. The model function has an approximately cos 2ϕ dependence (Jones *et al.* 1982) and as a result the sum of the

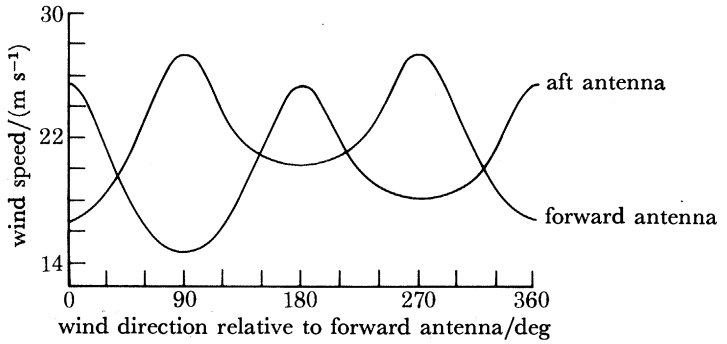

FIGURE 2. The locus of wind-vector solutions for two orthogonal noise-free σ° measurements. Directions given by the geophysical algorithm correspond to the intersections of the two curves, which in this case produces four possible directions, only one of which is correct. (From Jones *et al.* (1982).)

squares has several local minima. For a single noise-free σ° measurement the locus of solutions is a nearly sinusoidal curve in wind-vector space. For two orthogonal measurements (figure 2) the solutions correspond to the intersection of two curves and vary in number from two to four. These are the so-called directional aliases. They differ widely in direction but are approximately equal in magnitude.

Several methods have been proposed to remove the aliases from Seasat data. Wurtele *et al.* (1982) employ pattern recognition techniques to locate synoptic meteorological features by using SASS data alone and then select a preferred direction on the basis of streamline analysis. For 10 passes giving a total of 3476 comparisons with in-situ data, the correct direction was chosen on 70% of the occasions. A less subjective approach was adopted by Hoffman (1982), in an analysis of a single pass intersecting an intense mid-latitude depression, by direct minimization of an objective function that incorporated SASS and ship reports plus wind fields generated by a forecast model. Additional constraints that could be used are low-level winds derived from satellite cloud tracking (used by Endlich *et al.* 1982), correlation between low-level clouds and convergence in the inferred wind field, and surface pressure data. However, it is not clear that mesoscale features would be properly resolved. It has been suggested (O'Brien *et al.* 1982) that the problem might be alleviated in future scatterometers by the addition of extra antennae as currently planned for the E.S.A. satellite E.R.S.-1, which would reduce the number of aliases. Aliases with only two possible solutions are acceptable because they differ by nearly 180° in direction and so can be readily distinguished.

3. Assessment of accuracy

(*a*) *In-situ data*

After the premature end of the Seasat mission, several workshops were held at which winds calculated from the different geophysical algorithms were compared with various surface data sets. The latter included the Gulf of Alaska Seasat experiment (GOASEX) (J.P.L. 1979*a*, *b*),

high wind occasions (J.P.L. 1979*c*) and the Joint Air–Sea Interaction Experiment (JASIN) (J.P.L. 1980). Comparisons with GOASEX data revealed biases between antennae indicative of calibration problems and also inadequacies in the model functions, which were subsequently modified to minimize the discrepancies.

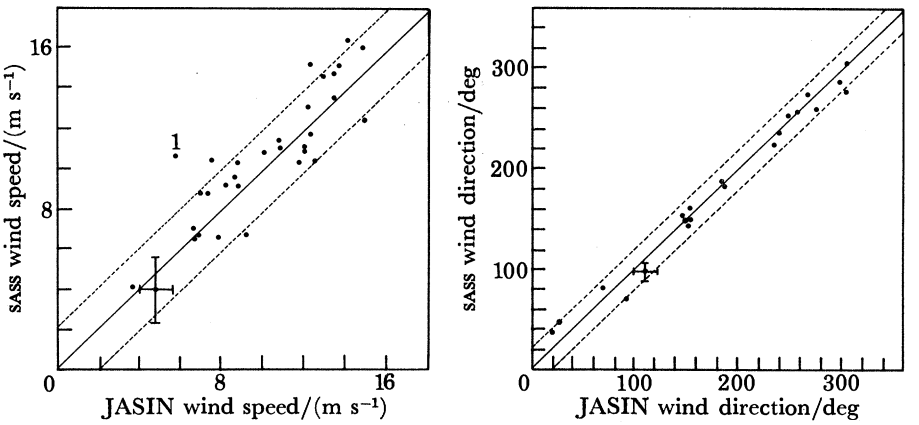

FIGURE 3. Comparison of scatterometer winds (w-7 algorithm) with JASIN winds (60 min means from ships and buoys) for 23 passes. Each point represents the mean of all comparisons for a particular satellite pass, typical standard deviations being indicated (point labelled 1: rev. 557, discussed in the text). Broken lines indicate the design specifications. Directions are with respect to true north. (From Allan & Guymer (1980).)

It was therefore necessary to assess the accuracy of these tuned model functions (now reduced to two, known as CWK and W-7) by using an independent high-quality data set. Fortunately, JASIN, a major international experiment, took place within Seasat's operational lifetime (Pollard *et al.* 1983). A number of ships and buoys sampled surface meteorological variables in a 200 km × 200 km area 300 km off NW Scotland at intervals from 1 min to 6 h. Careful comparisons were made between the sensors (Guymer 1983*a*; Brown *et al.* 1982) to produce an internally consistent data set in which interplatform differences in winds were less than 0.7 m s^{-1} (0.5 m s^{-1} for buoys) and less than 5°. The absolute accuracy of the wind speeds is difficult to determine. For convenience one buoy sensor was adopted as a standard to which all other data were corrected. Weller *et al.* (1983) have suggested that this may overestimate speeds by 10%, but such a view is not supported by comparison with aircraft-measured winds suitably corrected for height.

For the comparison two sets of SASS winds were generated for 23 passes by using the CWK and W-7 model functions. The passes were selected so as to give good spatial coverage of the JASIN area over as wide a range of wind speed as possible. Winds varied from 0 to 16 m s^{-1} with 83% distributed between 6 and 14 m s^{-1}. All measurements were corrected to give the 19.5 m neutral stability wind.

A detailed discussion of the results is given in J.P.L. (1980) and summaries appear in Jones *et al.* (1981*a*, 1982) and Schroeder *et al.* (1982*a*). An example of the comparisons of SASS winds (W-7 algorithm) with 60 min means of autologged ship and buoy data is given in figure 3. Most of the individual comparisons on which the figure is based were within the design specifications and the overall statistics showed that SASS winds were accurate to better than ± 1.7 m s^{-1} (W-7) and ± 1.5 m s^{-1} (CWK) in speed and ± 17° in direction for both algorithms.

However, some passes compared less favourably. The most striking was rev. 557 where wind

PHILOSOPHICAL TRANSACTIONS OF THE ROYAL SOCIETY A MATHEMATICAL, PHYSICAL & ENGINEERING SCIENCES

speeds were up to 15 m s^{-1} higher than measurements *in situ* for a small region near the southern corner of the JASIN triangle. Using JASIN surface and upper-air data and infrared satellite imagery, Guymer *et al.* (1981) were able to infer that a mid-level thunderstorm had affected the region at the time of the anomaly. It was concluded that the SASS winds were high because

TABLE 1. SASS MINUS IN-SITU WINDS FOR STORMS DATA SET, SASS-1 MODEL FUNCTION, VERTICAL AND HORIZONTAL POLARIZATIONS COMBINED

(All data except nadir (after Jones *et al.* 1982).)

hurricanes

in-situ wind speed/ (m s^{-1})	non-precipitating					precipitating				
		speed		direction			speed		direction	
	N	mean	σ	mean	σ	N	mean	σ	mean	σ
0–5	8	1.6	2.5	−2.2	15.3	7	5.8	0.8	3.8	19.2
5–10	128	0.7	1.7	0.7	19.6	24	1.9	2.1	5.2	28.2
10–15	215	1.0	1.7	0.7	14.4	45	0.5	1.5	3.9	18.3
15–20	53	1.0	1.2	−8.4	9.0	42	0.5	1.3	−0.2	19.3
20–25	0	—	—	—	—	46	−2.2	2.3	−3.2	1.94
>25	0	—	—	—	—	19	−7.8	6.0	−1.0	24.5
> 5	396	0.9	1.7	−0.5	16.0	176	−0.9	3.8	0.7	21.1

extratropical cyclone

	non-precipitating					precipitating				
		speed		direction			speed		direction	
	N	mean	σ	mean	σ	N	mean	σ	mean	σ
0–5	0	—	—	—	—	0	—	—	—	—
5–10	172	−0.3	2.6	−10.0	18.0	28	−0.1	3.0	−39.0	18.0
10–15	102	−3.2	1.7	−8.0	18.0	31	−2.7	2.2	−18.0	24.1
15–20	156	−1.7	2.4	−2.1	13.0	56	−2.1	1.3	−5.0	13.8
20–25	440	−1.7	2.4	−2.4	17.0	285	0.6	3.7	−7.2	21.0
>25	74	−3.4	2.5	−5.0	17.0	0	—	—	—	—
> 5	944	−1.7	2.6	−4.5	17.3	400	−0.2	3.4	−9.0	24.0

of the effect of raindrops on the sea surface or because of enhanced backscatter from the rain itself. This pass was excluded from the comparison statistics. On two other passes high standard deviations of the difference between the satellite and JASIN winds were found: both were frontal situations in which real horizontal wind-gradients contributed to the scatter.

Results with both algorithms indicated that agreement with *in situ* data was worst at 20–25° and 50–60° incidence angles, as also reported by Halberstam (1981). After the comparisons with the withheld JASIN data were completed it was decided to produce a new model function, SASS-1 (Boggs 1982*a*), tuned so as to minimize the differences. For most wind-speed–incidence angle categories the r.m.s. differences were significantly improved to better than ± 1.3 m s^{-1} and $\pm 17°$. Offiler (1981) extended these comparisons of the SASS-1 data set to all passes over JASIN and found similar results.

It should be noted that these figures include uncertainties in surface data that will arise not just from unremoved instrumental errors but also from unrepresentative sampling on the scale for which SASS winds are appropriate.

Neither GOASEX nor JASIN provided a validation of the upper wind-speed limit of the SASS and, owing to the short lifetime of Seasat, other planned calibration experiments were not held. Fortunately, coverage was obtained over three storms, an intense North Atlantic depression known as the *QEII* storm (see §4*a*) and two Pacific hurricanes, Fico and Ella, which have extended the comparisons. Results are summarized in table 1. A clear tendency for SASS

to underestimate winds over 20 m s^{-1} is evident in those regions of hurricanes with a high probability of precipitation. In part this is due to an inadequate attenuation correction in the intense rain bands because of the relatively poor SMMR resolution, and nonlinear brightness effects. It is also difficult to obtain meaningful comparisons in regions of large horizontal wind

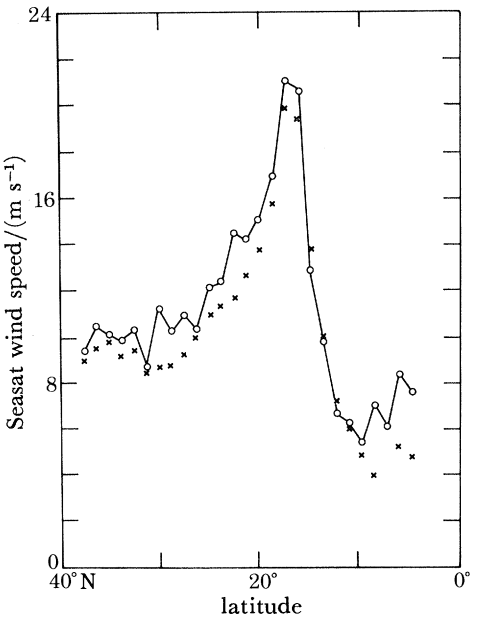

FIGURE 4. A comparison of SASS and SMMR wind speeds for Hurricane Fico, rev. 331. (From Wentz *et al.* (1982), with permission of the American Geographical Union.)

gradients near the hurricane centre. For the *QEII* storm the high wind-speed comparisons were in better agreement even when precipitation occurred. Rainfall in this extra-tropical feature was probably much less intense than in the hurricanes. Interestingly, there are no examples of anomalously high winds as in the JASIN thunderstorm, suggesting that backscatter is dominated by the wind-roughened surface or that the attenuation effects of rain outweigh any increased backscatter from the raindrops.

(*b*) *Comparisons with other Seasat sensors*

Wind speeds can also be obtained from the altimeter (Fedor & Brown 1982) and SMMR (Lipes 1982). Wentz *et al.* (1982) have compared SASS values with both instruments at nadir, and with the SMMR alone for the 100 km off-nadir where the instrument swaths overlap. From an analysis of four passes over the Gulf of Alaska Wentz *et al.* concluded that all three sensors agreed to within 2–3 m s^{-1} for winds between 2 and 10 m s^{-1}. However, at higher speeds the altimeter values are much lower. This is due to differences in the model functions rather than in the measured backscatter. I have found similar behaviour in a comparison of altimeter winds with surface data from JASIN and O.W.S. *Lima*.

In the off-nadir comparison Wentz *et al.* found that, in the mean, SMMR winds were 0.03 m s^{-1} greater than those from SASS, with a standard deviation of the difference about the mean of 1.42 m s^{-1}. The correlation between the two estimates was 0.95 for speeds between 2 and 20 m s^{-1}. Figure 4 shows SASS and SMMR winds from rev. 331, which passed through Hurricane Fico:

both sensors show a very similar along-track variation with a marked gradient of wind speed to the south of its centre. For the 27 cells considered the SMMR–SASS difference was 1.1 ± 1.1 m s^{-1}. It should be noted that this pass was early in Seasat's mission. Allan & Guymer (1982) have suggested that a change in the SMMR wind speed bias occurred on about rev. 900, which accounts for differences between JASIN and GOASEX SMMR comparisons. Nevertheless, these results confirm that SASS winds are accurate to within 2 m s^{-1}.

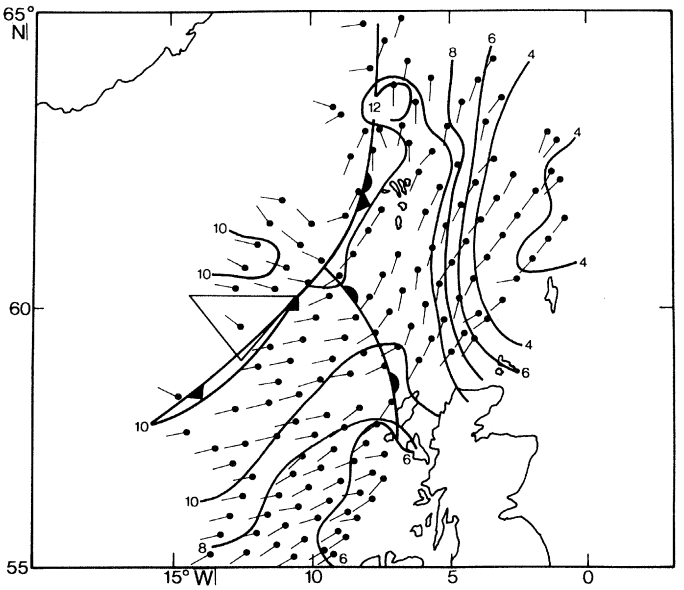

FIGURE 5. Scatterometer wind field for rev. 929, 23h11 G.M.T., 30 August 1978. Speed has been contoured in metres per second. (From Guymer *et al.* (1983).)

4. APPLICATIONS OF SEASAT SCATTEROMETER DATA

(*a*) *Synoptic mapping of surface wind velocity*

Two consecutive SASS passes (929 and 930) during the JASIN experiment gave coverage of a well defined occluding frontal system on 30/31 August 1978. Guymer *et al.* (1983) analysed the wind field on the first pass after removing the directional ambiguities in a manner similar to that of Wurtele *et al.* (1982) but also allowing routine pressure analyses every 6 h and JASIN surface winds to influence the choice of the preferred direction. The resulting wind field is shown in figure 5 with about 20% of the deduced wind vectors shown for clarity. A southerly flow ahead of the system strengthens near the warm front and veers to west-southwesterly in the warm sector. Across the cold front there is a marked change in direction of the flow. The position of the surface front on this occasion is quite clear even before the aliases are removed, being delineated by a change from the two-vector solution to the four-vector type. SASS data often allow the position of surface discontinuities to be determined more clearly than using conventional reports and infrared satellite imagery. This example illustrates the way in which the scatterometer enhances the spatial sampling of ocean winds. Further use of the data from this and the subsequent pass is made in §4*b*.

A more spectacular example of improved mapping of surface wind occurred on 9/10 September 1978, when coverage was obtained of an intense extra-tropical depression that under-

PHILOSOPHICAL TRANSACTIONS OF THE ROYAL SOCIETY A MATHEMATICAL, PHYSICAL & ENGINEERING SCIENCES

went rapid deepening to reach a minimum pressure of 960 mbar with 30 m s^{-1} winds leading to observed wave heights of 12 m (Guyakum 1980). This storm resulted in the loss of the trawler *Captain Cosmo* on 9 September and caused damage and injuries on the liner *Queen Elizabeth II* (*QEII*). Routine analysis seriously underestimated the intensity of the system, overestimating central pressures by about 20 mbar (though this involved neglecting one ship report which, in fact, turned out to be reliable) and underestimating surface winds by a factor of 2. A reanalysis of the occasion by Cane & Cardone (1981), who included SASS data, produced more consistent wind speeds and also placed the depression centre more accurately. Estoque & Fernandez-Partagas (1981), who analysed winds over the Indian Ocean, also found significant improvements in their analysis of the implied streamlines when the more uniform coverage due to SASS data was available.

(*b*) *Ekman pumping*

An important quantity when considering the response of the ocean to wind forcing or the effect of the atmospheric boundary layer on larger scales is the vertical motion arising from frictional convergence, W_f (often referred to as Ekman pumping), which is related to the wind stress curl by

$$W_f = (1/\rho f)\ \mathrm{curl}_z\ \boldsymbol{\tau}, \tag{2}$$

where

$$\mathrm{curl}_z\ \boldsymbol{\tau} = \frac{\partial \tau_{x0}}{\partial x} - \frac{\partial \tau_{x0}}{\partial y},$$

$$|\boldsymbol{\tau}| = \rho_{\mathrm{air}}\ U_*^2,$$

ρ is the density of air or water as appropriate, f is the Coriolis parameter, $\boldsymbol{\tau} = (\tau_{x0}, \tau_{y0})$ is the surface stress, which is related to the friction velocity, U_*, as shown. U_* values are included in the SASS data records, calculated from a constant flux layer model (Kondo 1975). (There is some hope (Liu & Large 1981) that it may be possible to relate the backscatter directly to the stress but insufficient high-quality flux data exist to produce a satisfactory algorithm.) The level to which the value of W_f refers is the boundary between the friction layer and the free atmosphere or ocean. Because W_f can be more easily compared with other quantities in the atmosphere (e.g. divergence measurements, cloud and weather types), the examples presented are for the air rather than the mixed layer of the ocean. Ekman pumping in the ocean is smaller by the ratio of the densities (*ca.* 1250).

Guymer *et al.* (1983) mapped the Ekman pumping deduced from SASS data in the vicinity of an occluding frontal system in the NE Atlantic. Figure 6 shows their results superimposed on a NOAA-5 infrared image obtained a few hours earlier. Maximum subsidence of 0.8 cm s^{-1} was found some 200–300 km ahead of the occlusion point and to the west of a ridge axis. Upward motion occurs along and just ahead of the surface front, especially near the occlusion point. Much of the warm-sector air is weakly descending in a region of relatively broken cloud as seen on the NOAA-5 infrared image. In general the distribution is consistent with the synoptic situation and the cloud cover. Taylor *et al.* (1982) investigated the horizontal variation of integrated water vapour, liquid water and rain rate derived from SMMR measurements on the same pass. Taken together, the results imply that warm, moist air ahead of the cold front is being lifted to produce rain just ahead of the occlusion point. The region with rain rates in excess of 0.4 mm h^{-1} is marked on figure 6. Guymer *et al.* (1983) found similar structure on the subsequent pass. Thus Ekman pumping appears to be related to larger-scale features of the free

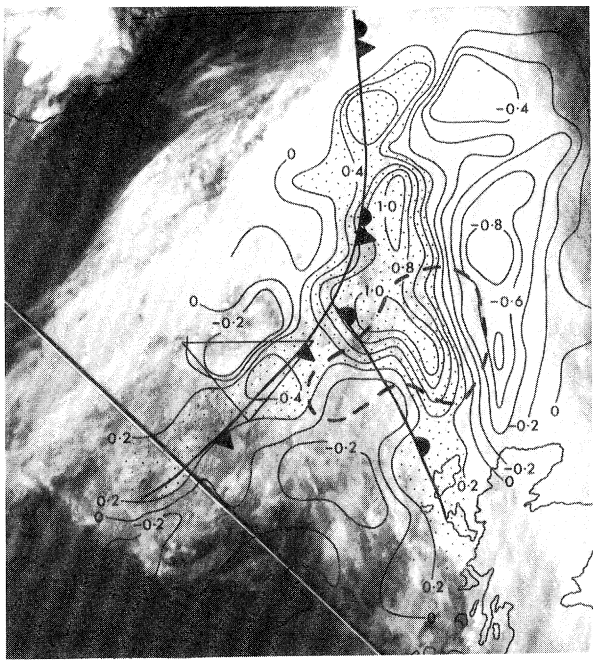

FIGURE 6. The distribution of vertical velocity (centimetres per second) at the top of the atmospheric friction layer calculated from the curl of the SASS wind stress, rev. 929, 23h11 G.M.T., 30 August 1978 (after Guymer *et al.* 1983). Data have been superimposed on a NOAA-5 infrared image (courtesy of University of Dundee) obtained at 18h35 G.M.T.

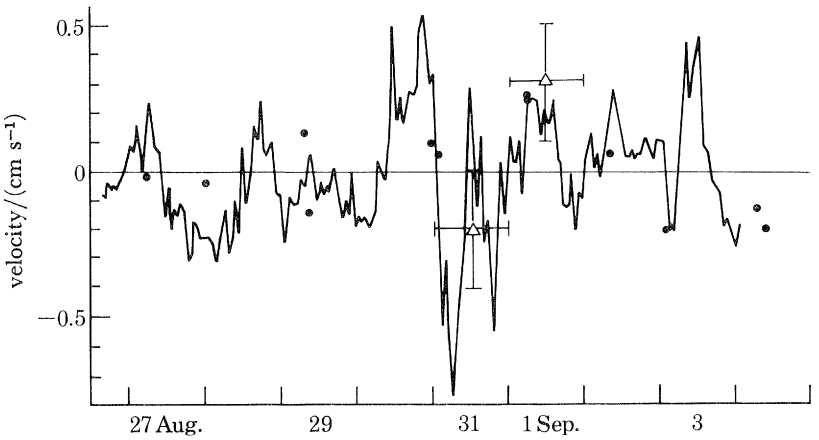

FIGURE 7. Estimates of the frictionally induced vertical velocity during JASIN Phase 2: solid line, from stresses derived from hourly ship winds; full circles, scatterometer-derived values. For comparisons the vertical motion resulting from the divergence method applied to radiosonde profiles is shown (triangles). (From Guymer & Taylor (1982).)

atmosphere. On another occasion (rev. 1006), however, Guymer (1983*b*) found little association between the distribution of W_f and the synoptic-scale features.

Several more passes during Phase 2 of JASIN were analysed in a similar way (Guymer & Taylor 1982), and mean values for the JASIN triangle have been plotted as a time series in figure 7. For comparison, hourly values have also been calculated by applying (2) to ship measurements of the surface wind at the corners of the JASIN triangle, after removal of inter-

platform biases based on careful comparison of results. The two sets of values agree within the uncertainty to be expected from errors in the wind measurements; they are also comparable with vertical velocities obtained from the divergence method applied to JASIN radiosonde winds at the triangle corners. This implies that most of the divergence in the atmospheric boundary layer was frictionally induced.

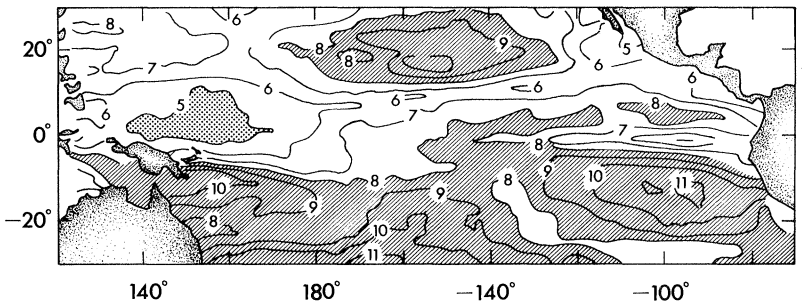

FIGURE 8. Mean wind-speed distribution (metres per second) in tropical Pacific derived from Seasat scatterometer measurements. (From Chelton & O'Brien (1982).)

Vertical motion at the base of the oceanic mixed layer has been inferred for the same period from heat budget considerations (T. Joyce, personal communication) and is an order of magnitude larger than can be accounted for by Ekman pumping. However, these values apply to a limited region near the southern corner of the triangle, where oceanic fronts (Pollard 1982) may have influenced the vertical velocities.

(*c*) *Time-averaged wind distribution*

The 3-month mean wind speed in the tropical Pacific derived by Chelton & O'Brien (1982) from SASS data is shown in figure 8. Off-nadir data from the right-hand side of the spacecraft have been used so that an atmospheric attenuation correction could be applied, and no attempt was made to retrieve the correct direction. Highest winds were located at about 20° N and 15° S, corresponding to the Trades; those in the southern (winter) hemisphere were stronger and more extensive in the zonal direction. The inter-tropical convergence zone is the light wind region just to the north of the equator and is also marked by a maximum in the vertically integrated water-vapour content (Chelton *et al.* 1981). Low-level convergence of moisture evaporated into the Trades at the Equator is an important mechanism in tropical disturbances and in the general circulation of the atmosphere. Scatterometer wind stresses, when combined with geostrophic currents from a satellite altimeter (Stewart 1982), will enable sea-surface currents to be monitored. Changes in the wind pattern also have important consequences for the variability of tropical ocean currents, e.g. the El Niño phenomenon and the Somali Current, and there is some evidence that there is a relation between current changes in the different tropical ocean basins and the atmosphere. Future scatterometer data have been identified as an important component of a proposed programme (Tropical Ocean and Global Atmosphere (C.C.C.O. 1982)) to study such features.

Chelton & O'Brien (1982) noted a discrepancy between SASS and altimeter winds (latter biased low) for this 3 month period and hypothesized that it was due to effects of high atmospheric water content and sea surface temperature compared with their values at the (mid-latitude) calibration sites. It seems to us more likely, in view of §3*b*, that the difference is due

to errors in the altimeter wind algorithm above 10 m s^{-1} combined with sampling errors resulting from its narrow swath.

An example of the wind speeds obtained for a large portion of the world ocean in a 2 day period has been produced by Schroeder *et al.* (1982*b*). In addition to the features described above, several mid-latitude storms can be identified. High wind speeds are also indicated south of 60° S but these are not real, being caused by high backscatter from sea ice, as also found by Boggs (1982*b*). Backscatter measurements at nadir from the Seasat altimeter have been analysed by Guymer & Kennett (1983) to delineate the sea-ice boundary more accurately. A combination of altimeter and scatterometer data is useful for monitoring sea-ice extent.

(*d*) *Interpretation of synthetic aperture radar imagery*

SAR imagery has revealed a wealth of interesting features at the ocean surface (Vesecky & Stewart 1982) that have been identified with surface gravity waves, internal waves, natural and man-made slicks, streaks, etc. The mechanisms by which these are imaged are not fully understood but since the instrument basically measures the backscatter from short-wavelength (*ca.* 30 cm) surface roughness elements, which are then modulated in some way by larger scales, wind speed must be important. The overlap of SASS and SAR swaths allows an investigation of the image characteristics in relation to the wind field on scales of 50 km and greater.

Beal (1981) verified from aircraft and SASS winds that large dark regions on SAR imagery of Chesapeake Bay, corresponding to low backscatter, were associated with light winds. Allan & Guymer (1981, 1983) analysed SASS wind-fields for a number of SAR images in the NE Atlantic and concluded that the transition between zero and measurable backscatter occurred at 3 m s^{-1} and was commonly less than 100 m wide. At winds just above the threshold, horizontal variations in image intensity appeared to be more pronounced than in strong winds. Surface gravity waves with wavelengths and directions consistent with surface data were sometimes visible for both cross-track and along-track orientations of the wave-crests, provided that winds were not too strong. For winds greater than 15 m s^{-1} there was a tendency for streaks to be imaged at the expense of waves (figure 9). These streaks were within $\pm 10°$ of being parallel to the SASS winds, had a spacing of 2–3 km and extended over hundreds of kilometres, suggesting that, primarily, atmospheric forcing was modulating the surface backscatter. These observations, together with the fact that neither SAR (Jones *et al.* 1981*b*) nor SASS backscatter saturates at the low wind speeds (a few metres per second) that theory (Phillips 1977) predicts for short ocean waves, raise important questions about what causes the measured backscatter. One possibility is that the proportion of the sea surface covered by ripples is dependent on wind speed; another is that bubbles at the surface, caused by wave-breaking, are contributing to the backscatter. At high wind speeds, foam patches persist for periods of a minute or longer, cover large areas and are not necessarily organized on the scale of the waves. It is suggested that these mechanisms compete against others (tilt, hydrodynamic and orbital velocity) that have been proposed to explain imaging of surface gravity waves (Tucker, this symposium).

(*e*) *Other applications*

Numerical weather prediction and storm-surge models require sea-level pressure analyses Endlich *et al.* (1982) have demonstrated the feasibility of deriving pressure fields from SASS winds. Wind vectors were computed on a regular grid mesh from three consecutive passes; the pressure distribution was calculated from the balance equation (which in its simplest form

PHILOSOPHICAL TRANSACTIONS OF THE ROYAL SOCIETY A MATHEMATICAL, PHYSICAL & ENGINEERING SCIENCES

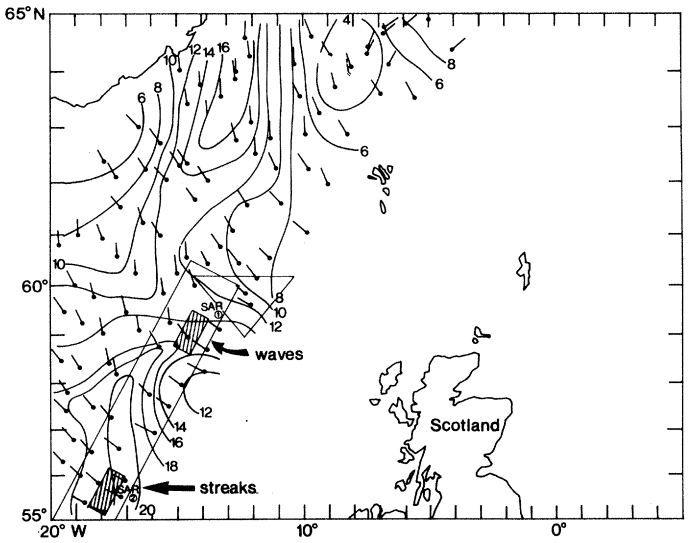

FIGURE 9. Scatterometer wind-velocity field (metres per second) on rev. 1087, 11 September 1978. Locations of two synthetic aperture radar images that have been analysed are also shown. (From Allan & Guymer (1983).)

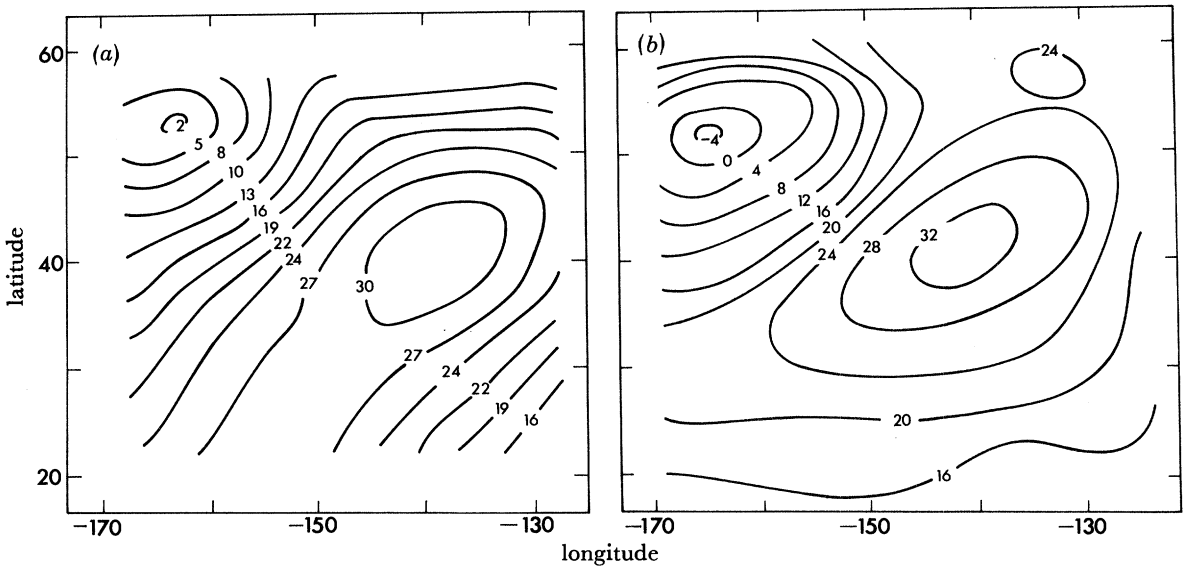

FIGURE 10. Surface pressure field over northern Pacific Ocean as the departure from 1000 mbar on 17 July 1978. (*a*) Balanced values computed from the non-divergent component of scatterometer winds between 12h00 and 16h00 G.M.T.; (*b*) corresponding National Meteorological Centre analysis for 12h00 G.M.T. (From Endlich *et al.* (1981), by permission of the American Meteorological Society.)

reduces to the geostrophic relation) by using the non-divergent component of the wind field. Absolute values were obtained from surface-measured pressure at two locations. The resulting pressure field is shown in figure 10 with the conventional analysis for comparison. The correlation coefficient between the two is 0.91 and the r.m.s. difference is 4.4 mbar; some of the error is due to changes occurring during the 300 min needed to obtain the SASS data.

The incorporation of global SASS data into numerical weather forecasts was investigated for a 2 day period by Yu and McPherson (1981). Largest differences were in the Southern

Hemisphere and extended up to the tropopause. Comparison with cloud imagery suggested that the inclusion of the SASS data improved the forecast.

Wind-wave forecasting models should also benefit from scatterometer winds. In the *QEII* storm, wave heights were forecast to be 3 m but were actually 12 m. The discrepancy was mainly due to underestimation of the wind speed.

5. Concluding remarks

Comparisons with reliable surface data have shown that the Seasat scatterometer produced useful estimates of near-surface wind velocity and that between 3 and 16 m s^{-1} they were well within the design specifications of ± 2 m s^{-1} and 20°. The application of these data in a number of scientific and operational areas has been described. It is still clear that many questions about radar backscatter from the ocean remain to be answered, especially the causes of its wind-speed dependence above a few metres per second. At present it seems doubtful whether the wind scatterometer on the European satellite, ERS-1, will achieve a similar accuracy to the SASS because there are two important differences:

(i) it will operate at 5.3 GHz (C-band), where σ° is known to be much less sensitive to the wind;

(ii) ERS-1 will not carry a broad-swath microwave radiometer from which an atmospheric attenuation correction can be obtained. Although attenuation is less severe at C-band it may not be negligible in regions of high rain-rate, especially in view of (i).

The support of the University of Washington is gratefully acknowledged.

References

Allan, T. D. & Guymer, T. H. 1980 *Int. J. Remote Sensing* **1**, 261–267.
Allan, T. D. & Guymer, T. H. 1981 In *Proc. EARSeL–E.S.A. Symp., Voss* (ESA-SP-167), pp. 119–127.
Allan, T. D. & Guymer, T. H. 1983 *Int. J. Remote Sensing.* (In the press.)
Beal, R. C. 1981 In *Spaceborne synthetic aperture radar for oceanography* (ed. R. C. Beal, P. de Leonibus & I. Katz), pp. 110–127. Baltimore, Maryland: Johns Hopkins Press.
Boggs, D. H. 1982*a* *J.P.L. N.T.I.S. P.D.* no. 622-230. (44 pages.) Jet Propulsion Laboratory, Pasadena.
Boggs, D. H. 1982*b* *J.P.L. Report* no. 622-232. Jet Propulsion Laboratory, Pasadena.
Born, G. H., Lame, D. B. & Rygh, P. J. 1981 In *Oceanography from space* (ed. J. F. R. Gower), pp. 3–14. New York: Plenum.
Bradley, G. A. 1971 Ph.D. thesis, University of Kansas.
Brown, R. A., Cardone, V. J., Guymer, T., Hawkins, J., Overland, J. E., Pierson, W. J., Peteherych, S., Wilkerson, J. C., Woiceshyn, P. M. & Wurtele, M. 1982 *J. geophys. Res.* **87** (C5), 3355–3364.
Businger, J. A. & Charnock, H. 1983 *Phil. Trans. R. Soc. Lond.* A **308**, 445–449.
Cane, M. A. & Cardone, V. J. 1981 In *Oceanography from space* (ed. J. F. R. Gower), pp. 587–595. New York: Plenum.
Cardone, V. J. 1970 *New York Univ. Report* no. TR 69-1. University Heights, New York.
C.C.C.O. 1982 *Report of the Joint C.C.C.O./J.S.C. Study Conference on Large-Scale Oceanographic Experiments in the World Climate Research Programme.* (IOC/INF-507.)
Chelton, D. B., Hussey, K. J. & Parke, M. E. 1981 *Nature, Lond.* **294**, 529–532.
Chelton, D. B. & O'Brien, J. J. 1982 *Trop. Ocean–Atmos. Newsl.* **11**, 3–4.
Claasen, J. P., Fung, A. K., Moore, R. K. & Pierson, W. J. 1972 In *IEEE Int. Conf. Engineering in the Ocean Environment, Newport, R.I., U.S.A.*, pp. 180–185.
Cowan, E. W. 1946 *M.I.T. Radiation Lab., Rep.* no. 870. Cambridge, Massachusetts.
Daley, J. C. 1973 *J. geophys. Res.* **78**, 7823–7833.
Dome, G. J., Fung, A. K. & Moore, R. K. 1977 In *Proc. URSI Commission F, La Baule, France*, 28 *April to* 6 *May*, pp. 591–596.

Endlich, R. M., Wolf, D. E., Carlson, C. T. & Maresca, J. W. Jr 1981 *Mon. Weath. Rev.* **109**, 2009–2016.
Estoque, M. A. & Fernandez-Partagas, J. 1981 *Tellus* **33**, 463–475.
Fedor, F. S. & Brown, G. S. 1982 *J. geophys. Res.* **87** (C5), 3385–3395.
Grant, C. R. & Yaplee, B. S. 1957 *Proc. Inst. Radio Engrs* **45**, 976.
Grantham, W. L., Bracalente, E. M., Jones, W. L. & Johnson, J. W. 1977 *IEEE J. ocean. Engng* **OE-2**, 200–206.
Guignard, N. W., Ransone, J. T. Jr & Daley, J. C. 1971 *J. geophys. Res.* **76**, 1525.
Guymer, T. H. 1983*a* I.O.S. internal report (in preparation).
Guymer, T. H. 1983*b* In *Satellite microwave remote sensing* (ed. T. D. Allan). Ellis Horwood.
Guymer, T. H., Businger, J. A., Jones, W. L. & Stewart, R. H. 1981 *Nature, Lond.* **294**, 735–737.
Guymer, T. H., Businger, J. A., Katsaros, K. B., Shaw, W. J., Taylor, P. K., Large, W. G. & Payne, R. E. 1983 *Phil. Trans. R. Soc. Lond.* A **308**, 253–273.
Guymer, T. H. & Kennett, M. J. 1983 In preparation.
Guymer, T. H. & Taylor, P. K. 1983 In *Proceedings of the Joint C.C.C.O./J.S.C. Study Conference on Large-Scale Oceanographic Experiments in the World Climate Research Programme, Tokyo*, 10–21 *May* 1972. (In the press.)
Gyakum, J. R. 1980 In Preprints of Eighth Weather Forecasting and Analysis Conference, A.M.S., Boston, pp. 23–28.
Halberstam, I. 1981 *J. geophys. Res.* **86**, 6599–6606.
Hoffman, R. N. 1982 *Mon. Weath. Rev.* **110**, 434–445.
Johnson, J. W., Williams, L. A. Jr, Bracalente, E. M., Beck, F. B. & Grantham, W. L. 1980 *IEEE J. ocean. Engng* **OE-5**, 138–144.
Jones, W. L., Boggs, D. H., Bracalente, E. M., Brown, R. A., Guymer, T. H., Chelton, D. & Schroeder, L. C. 1981*a* *Nature, Lond.* **294**, 704–707.
Jones, W. L., Delnore, V. E. & Bracalente, E. M. 1981*b* In *Spaceborne synthetic aperture radar for oceanography* (ed. R. C. Beal, P. de Leonibus & I. Katz), pp. 87–94. Baltimore, Maryland: Johns Hopkins Press.
Jones, W. L. & Schroeder, L. C. 1978 *Bound. Layer Met.* **13**, 133–149.
Jones, W. L., Schroeder, L. C., Boggs, D. H., Bracalente, E. M., Brown, R. A., Dome, G. J., Pierson, W. J. & Wentz, F. J. 1982 *J. geophys. Res.* **87** (C5), 3297–3317.
Jones, W. L., Schroeder, L. C. & Mitchell, J. L. 1977 *IEEE J. ocean. Engng* **OE-2**, 52–60.
Jones, W. L., Wentz, F. J. & Schroeder, L. C. 1978 *AIAA J. Spacecraft Rockets* **15**, 368–374.
J.P.L. 1979*a* Rep. no. 622-101. Jet Propulsion Laboratory, Pasadena.
J.P.L. 1979*b* Rep. no. 622-107. Jet Propulsion Laboratory, Pasadena.
J.P.L. 1979*c* Rep. no. 622-210. Jet Propulsion Laboratory, Pasadena.
J.P.L. 1980 *J.P.L. Publication* no. 80–62. Jet Propulsion Laboratory, Pasadena.
Kerr, D. E. 1951 In *Propagation of short radio waves.* New York: McGraw-Hill.
Kondo, J. 1975 *Bound.-Layer Met.* **9**, 91–112.
Lipes, R. G. 1982 *J. geophys. Res.* **87** (C5), 3385–3395.
Liu, W. T. & Large, W. G. 1981 *J. phys. Oceanogr.* **11**, 1603–1611.
Mitsuyasu, H. 1977 *J. phys. Oceanogr.* **7**, 882–891.
Moore, R. K., Birrer, I. J., Bracalente, E. M., Dome, G. J. & Wentz, F. J. 1982 *J. geophys. Res.* **87** (C5), 3337–3354.
Moore, R. K. & Fung, A. K. 1979 *IEEE Proc.* **67**, 1504–1521.
Moore, R. K. & Young, J. D. 1977 *IEEE J. ocean. Engng* **OE-2**, 309–317.
O'Brien, J. J. (ed.) 1982 *Scientific opportunities using satellite wind stress measurements over the ocean.* Fort Lauderdale, Florida: Nova University/N.Y.I.T. Press.
Offiler, D. 1981 Met. O.19 Branch Memorandum no. 64 (unpublished). Meteorological Office, Bracknell.
Phillips, O. M. 1977 *The dynamics of the upper ocean.* New York: Cambridge University Press.
Pierson, W. J., Cardone, V. J. & Greenwood, J. A. 1974 *The applications of Seasat-A to meteorology* (Technical Report, City University of New York.)
Pierson, W. J. & Stacy, R. A. 1973 *N.A.S.A. Contractor Rep.* no. CR-2247. (128 pages.)
Pollard, R. T. 1982 JASIN News no. 25, unpublished manuscript.
Pollard, R. T., Guymer, T. H. & Taylor, P. K. 1983 *Phil. Trans. R. Soc. Lond.* A **308**, 221–230.
Robinson, A. R. (ed.) 1963 *Wind-driven ocean circulation.* New York: Blaisdell.
Schroeder, L. C., Boggs, D. H., Dome, G. J., Halberstam, I. M., Jones, W. L., Pierson, W. J. & Wentz, F. J. 1982*a* *J. geophys. Res.* **87** (C5), 3318–3336.
Schroeder, L. C., Grantham, W. L., Mitchell, J. L. & Sweet, J. L. 1982*b* *IEEE J. ocean. Engng* **OE-7**, 3–14.
Stewart, R. H. 1983 In *Proceedings of the Joint C.C.C.O./J.S.C. Study Conference on Large-Scale Oceanographic Experiments in the World Climate Research Programme, Tokyo*, 10–21 *May* 1972. (In the press.)
Taylor, P. K., Guymer, T. H., Katsaros, K. B. & Lipes, R. G. 1983 In *Proc. Symp. Variations in the Global Water Budget, Oxford*, 10–15 *August* 1981. (In the press.)
Vesecky, J. F. & Stewart, R. H. 1982 *J. geophys. Res.* **87** (C5), 3397–3430.
Weller, R. A., Large, W. G., Payne, R. E. & Zenk, W. 1983 *J. appl. Met.* (Submitted.)
Wentz, F. J., Cardone, V. J. & Fedor, L. S. 1982 *J. geophys. Res.* **87** (C5), 3378–3384.

PHILOSOPHICAL TRANSACTIONS OF THE ROYAL SOCIETY A MATHEMATICAL, PHYSICAL & ENGINEERING SCIENCES

Wurtele, M. G., Woiceshyn, P. M., Peteherych, S., Borowski, M. & Appleby, W. S. 1982 *J. geophys. Res.* **87** (C5), 3365–3377.

Yu, T. W. & McPherson, R. D. 1981 Presented at Fifth Conference on Numerical Weather Prediction, 2–6 November 1981, Monterey, California.

PHILOSOPHICAL TRANSACTIONS OF THE ROYAL SOCIETY A MATHEMATICAL, PHYSICAL & ENGINEERING SCIENCES

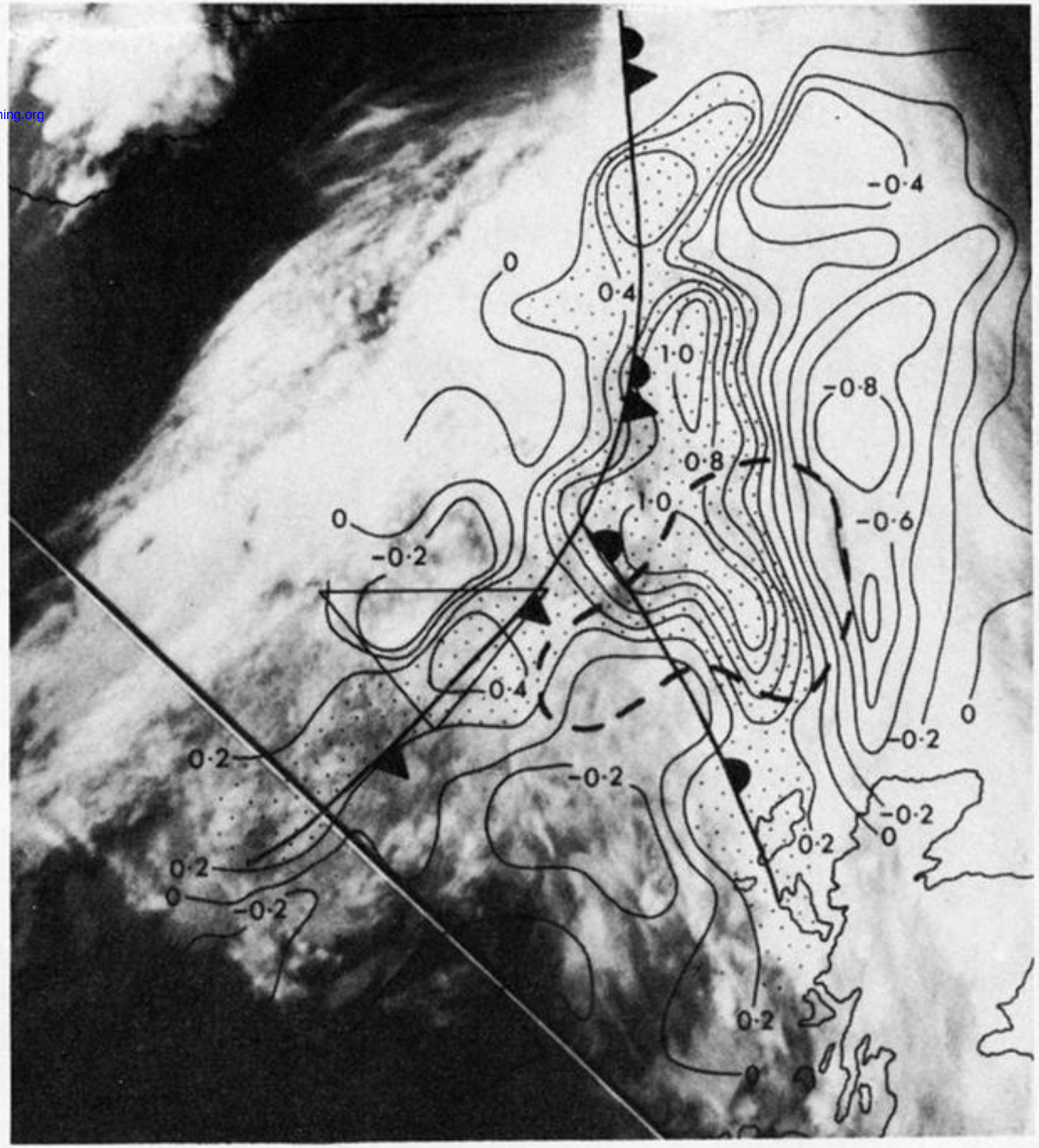

GURE 6. The distribution of vertical velocity (centimetres per second) at the top of the atmospheric friction layer calculated from the curl of the SASS wind stress, rev. 929, 23h11 G.M.T., 30 August 1978 (after Guymer *et al.* 1983). Data have been superimposed on a NOAA-5 infrared image (courtesy of University of Dundee) obtained at 18h35 G.M.T.

PHILOSOPHICAL TRANSACTIONS OF THE ROYAL SOCIETY A MATHEMATICAL, PHYSICAL & ENGINEERING SCIENCES